Chasing PtO$_x$ species in ceria supported platinum during CO oxidation extinction with correlative operando spectroscopic techniques

(article starts on next page)

Chasing PtO$_x$ species in ceria supported platinum during CO oxidation extinction with correlative *operando* spectroscopic techniques

Mengqiao Di [a,*], Kerry Simmance [b], Andreas Schaefer [a], Yanyue Feng [a], Felix Hemmingsson [a], Magnus Skoglundh [a], Tamsin Bell [b], David Thompsett [b], Lucy Idowu Ajakaiye Jensen [c], Sara Blomberg [c], Per-Anders Carlsson [a,1]

[a] *Competence Centre for Catalysis, Department of Chemistry and Chemical Engineering, Chalmers University of Technology, 412 96 Gothenburg, Sweden*
[b] *Johnson Matthey Technology Centre, Blounts Court, Sonning Common, Reading RG4 9NH, UK*
[c] *Department of Chemical Engineering, Lund University, 221 00 Lund, Sweden*

ABSTRACT

Industrially relevant, highly dispersed, Pt/ceria and reference Pt/alumina catalysts with narrow Pt particle size distributions have been prepared, characterised *ex situ* and studied for CO oxidation by *operando* infrared and X-ray absorption spectroscopy. At high CO conversions, spectator CO ad-species on ionic platinum are observed while the CO oxidation proceeds on Pt particles in a high oxidation state exhibiting significant Pt—O coordination. During the protracted catalytic extinction, the CO coverage builds up gradually while the Pt oxidation state and Pt—O coordination remain high because of interactions with ceria. The observed CO oxidation at high CO coverage is suggested to involve sites at the platinum-ceria boundary that cannot be CO self-poisoned. This behaviour is in stark contrast to that of Pt/alumina, which shows removal of platinum oxides formed during CO oxidation and the classical drop in catalytic activity caused by rapid CO self-poisoning when reaching a critical temperature.

© 2022 The Author(s). Published by Elsevier Inc. This is an open access article under the CC BY license (http://creativecommons.org/licenses/by/4.0/).

1. Introduction

Heterogeneous catalyst technologies for abatement of urban air pollutants, improvement of indoor air quality and purification of chemical feedstocks and fuels depend on further development of the CO oxidation functionality [1–3]. One example concerns automotive exhaust aftertreatment catalysts for emerging vehicle powertrains. Because of their higher engine combustion efficiency and/ or electrical hybridisation, the exhausts have low temperatures and low (latent) combustion heat that can be utilised to increase the temperature in the catalytic converter. Although significant, the challenge is not only to abate emissions during the cold-start period [4] but also to prevent catalytic extinction upon vehicle deceleration, engine start-and-stop operation and switching between modes of propulsion [5]. This stresses the need for catalysts that can operate efficiently at low temperatures, ideally being active for CO oxidation at ambient conditions.

Among the platinum-group metals active for CO oxidation one finds Pt to be the more robust element for use in applications. It resists carbon dioxide, water and sulfur components relatively well and can be sufficiently stablised towards sintering by being dispersed onto a suitable support. The support is commonly a metal oxide [6–8]. The selection of the metal oxide is crucial because it influences not only the dispersion of platinum particles but also their catalytic properties and overall catalytic performance. Silica and alumina are often referred to as inactive supports as they cannot be reduced reversibly whereas ceria with its dynamic redox properties, high oxygen mobility and strong interaction with platinum is called an active support that also can take part in the catalytic reaction [9–11].

The oxidation of CO over Pt catalysts typically exhibits bistable kinetics [12–14]. At low temperature, and/or O$_2$ concentration, the CO oxidation rate is low because of CO self-poisoning. Upon increasing the temperature, and/or O$_2$ concentration, a critical point may be reached at which a so-called first order kinetic phase transition occurs [15]. This means a drastic change of the qualitative behaviour of the kinetics such that adsorbed CO is rapidly reacted away, adsorbed O becomes the main surface species and the catalytic reaction proceeds with a high rate [12,16,17]. Analo-

---

gously, decreasing the temperature, and/or O_2 concentration, may lead to a sudden CO self-poisoning, when another critical point is reached, with the corresponding low reaction rate [12–15]. The bistable behaviour is captured by the common three-step mechanism including competitive reversible adsorption of CO (associative) and O_2 (dissociative), and rapid reaction between adsorbed CO and O into CO_2 that immediately desorbs at temperatures above room temperature [18,19]. At the conditions of exhaust aftertreatment, platinum oxide formation/removal may complicate the reaction kinetics [20,13] by giving rise to, for example, kinetic oscillations [21]. The oxide formation during CO oxidation conditions is seldom complete but rather results in partial oxidation of the Pt particles [20] thus containing coexisting Pt—Pt and Pt—O species whereof the latter has been reported to represent a defected oxide (shorter Pt—O bond length) as compared to bulk platinum oxide [22]. For platinum dispersed onto ceria, surface processes over the platinum-ceria boundary add to the mechanistic complexity [14,23]. Using model systems, sites at the Pt—O—Ce boundary have been proposed to be important although the role of PtPt—O species in the reaction mechanism is still an open question [24].

The significance of reactions on interface sites at the Pt-support boundary depend on the Pt particle size and support material. On the one hand, for large faceted particles, the kinetics is dominated by elementary processes occurring on communicating facets. In essence, rate data from Pt single crystal studies suffice to describe the kinetics on these facets unless platinum oxide develops [12,13]. On the other hand, for atomically dispersed Pt on ceria, the activity is low and CO adsorbed on such sites has been shown to be spectator species [25,26]. For a recent review on relevant single-atom catalysts see Ref. [27]. For small nanoparticles, say between 1 and 5 nm, the kinetics clearly depends on the interacting support [28,29] although for cluster sized Pt species comprised of Pt—OPt—Pt entities, the support has been suggested to have less influence on the catalytic properties [26]. This demonstrates the structure gap. It can be particularly complex for industrial catalysts, containing a variation of particle sizes, for which the catalyst efficiency and structural dynamics driven by the surface processes hardly can be represented by model catalysts but remain to be resolved for the actual system under consideration.

Thanks to the rich scientific literature, the CO oxidation reaction provides a means for understanding catalytic materials by being a prototypical reaction that can be followed by advanced analytical methods. The present aim is to understand the CO oxidation extinction process over industrially relevant catalysts. Special attention is paid to how ceria modifies the evolution of PtO_x species in small ($\approx$1 nm) Pt particles during catalytic CO oxidation extinction as compared to Pt/alumina reference catalyst. The catalysts have been prepared by wet chemical methods suitable for industrial production, evaluated by chemical flow reactor measurements and studied in detail using *operando* infrared and X-ray absorption spectroscopy. Thereby the evolution of surface species, chemical state and structural dynamics could be related to global kinetics of CO oxidation.

2. Experimental

2.1. Preparation and basic characterization of the catalysts

The catalysts were prepared by incipient wetness impregnation using platinum salts followed by drying and calcination at 500 °C in static air.

The specific surface area (SSA) of the as prepared catalysts was determined from N_2 physisorption at 77 K using a Tristar 3000 (Micromeritics) instrument and employing the Brunauer-

Emmett-Teller (BET) equation. Prior to the adsorption measurements, the samples were dried overnight at 250 °C under a flow of N_2.

The number of surface Pt atoms was determined from CO chemisorption at 35 °C using an ASAP2020 Plus (Micromeritics) instrument. Around 200 mg catalyst was placed between two quartz wool wads in the bottom of a quartz U-tube encased in a high-temperature furnace. The Pt/alumina catalyst was pretreated at 500 °C with 100 vol.% O_2 for 1 h followed by 100 vol.% H_2 also for 1 h. Then, the sample was cooled in He to the chemisorption temperature. The Pt/ceria catalyst was pretreated with 100 vol.% O_2 at 500 °C for 1 h, cooled to 250 °C in presence of O_2 and exposed to 100 vol.% H_2 for 1 h. Then, the sample was cooled to 35 °C in H_2 and exposed to 100 vol.% CO_2 for 1 h. Subsequently, the sample was treated with 100 vol.% O_2 for 30 min and then 100 vol.% H_2 for 30 min. 10–20 min evacuation was used in between introducing different gases. After the pretreatments, the samples were evacuated for 20 min and then CO chemisorption was carried out by dosing 100 vol.% CO from 13 to 80 kPa for Pt/alumina and to 93 kPa for Pt/ceria. The specific Pt area was determined from the number of surface Pt atoms assuming that one CO molecule binds to one surface Pt atom as determined by infrared spectroscopy [30] and a Pt cross-sectional area of 8 $Å^2$. Further, the Pt dispersion and mean Pt particle size were calculated from the number of surface Pt atom and measured Pt loading assuming hemispherical particle shape.

The crystalline phases of the catalysts were determined by powder X-ray diffraction (PXRD) using a D8 Advance diffractometer (Bruker) equipped with a Cu-K_α X-ray source (1.5418 Å) and a Lynx-eye energy dispersive detector. Diffractograms were recorded under ambient conditions in the 2θ range from 20° to 90° with an incremental step of 0.02° and a dwell time of 1.8 s at each step. The Scherrer equation was used to calculate crystallite sizes considering the full width at half-maximum (FWHM) of four major diffraction peaks at 32° (220), 37° (331), 46° (400) and 67° (440) for Pt/alumina and 29° (111), 33° (200), 47° (220) and 56° (311) for Pt/ceria.

The Pt particles were imaged with high-resolution transmission electron microscopy (HRTEM) using an Tecnai T20 microscope (FEI) equipped with a LaB_6 filament operating at 200 kV and a high-angle annular dark-field STEM detector as well as with scanning transmission electron microscopy (STEM) and energy-dispersive X-ray (EDX) spectroscopy using an Titan 80–300 microscope (FEI) equipped with a field emission gun operating at 300 kV. The preparation of the specimen included dispersing the catalyst sample in ethanol with subsequent ultrasonication. Thereafter, a droplet of the suspension was loaded onto a holey carbon film on a copper grid. The recorded images were analysed by ImageJ [31] to reveal the Pt particle size distribution.

2.2. Temperature programmed reduction and reaction

Hydrogen temperature programmed reduction (H_2-TPR) measurements were carried out using a Sensys differential scanning calorimeter (Setaram) system including a vertical quartz tube, with an inner porous sintered quartz frit with a diameter of 4 mm holding the sample, inside a controllable heated compartment. The gas flow was composed by individual mass flow controllers (Bronkhorst) and the effluent gas was analysed with a Hiden HPR-20 QUI mass spectrometer. Using the sieved fraction of 40–80 μm, the loaded amount of Pt/alumina and Pt/ceria was 50.6 and 19.9 mg, respectively. The catalyst was pre-oxidised with 20 vol.% O_2 at 250 °C for 30 min, then cooled with a ramp rate of 5 °C/min to room temperature (RT) in Ar. After 60 min, the catalyst was exposed to 1 vol.% H_2 for 20 min at RT. The H_2-TPR measure-

ment was then carried out by heating the temperature with a rate of 5 °C/min to 800 °C in the presence of 1 vol.% H_2.

The catalyst performance was evaluated using a vertical fixed-bed powder reactor made of a 33 cm long quartz tube with an inner and outer diameter of 4 and 6 mm, respectively. The reactor was surrounded by a metal coil for resistive heating and insulated by a layer of quartz wool. The feed gas was composed by a set of mass flow controllers (Bronkhorst). The inlet gas temperature was measured by a type K thermocouple located 1–2 mm above the sample. The effluent gas was analysed using a Hiden HPR-20 mass spectrometer following the m/e ratios 28 (CO), 32 (O_2) and 44 (CO_2). Before loading the catalyst into the reactor, the catalyst sample was sieved and the fraction 40–80 μm was collected and diluted with grinded cordierite (Corning) sieved to the fraction 300–355 μm. The catalyst weight was around 6 mg for Pt/ceria and for Pt/alumina. The total weight of the bed was around 180 mg and thus the catalyst-to-cordierite mass ratio was about 1:30. The catalytic activity for CO oxidation was evaluated by temperature programmed reaction measurements following the catalytic extinction process. The total gas flow was fixed at 400 ml/min, which corresponds to a gas hourly space velocity of 127000 h^{-1}. The CO oxidation measurements were carried out using either 0.5, 0.2 or 0.05 vol.% CO with 2 vol.% O_2 and Ar as carrier gas. The following temperature cycle was repeated three times: the temperature was increased to 250 °C and maintained for 50 min for the first extinction cycle and for 20 min for the remaining 2 cycles, then decreased to 50 °C with a rate of 5 °C/min.

2.3. Operando spectroscopy

2.3.1. Diffuse reflectance infrared Fourier transform spectroscopy

Adsorbate speciation during adsorption/desorption and oxidation of CO was done with diffuse reflectance infrared Fourier transform spectroscopy (DRIFTS) using a VERTEX 70 FTIR spectrometer (Bruker) equipped with a nitrogen coo-led MCT detector and a high-temperature stainless steel reaction chamber (Harrick) with CaF_2 windows. The chamber was mounted inside a Praying Mantis mirror accessory (Harrick). One type K thermocouple was used to measure the temperature underneath the sample holder (gas inlet) and another thermocouple was bended and inserted as to measure the temperature inside the catalyst bed. A thin layer of catalyst was placed on a bed of KBr that filled the holder. Individual mass flow controllers (Bronkhorst) were used to compose the feed gas. The total flow was 100 ml/min and constant. IR spectra in the range 4400–400 cm^{-1} were collected with a spatial resolution of 1 cm^{-1}. Using a 6 mm aperture and 20 kHz scanner velocity, background and sample spectra were recorded by taking an average of 100 and 50 scans, respectively.

Prior to adsorption and oxidation of CO, the catalyst was heated to 211 °C and treated with 5 vol.% O_2 for 40 min followed by 1 vol.% H_2 for another 30 min using Ar as carrier. Upon reaching a low and stable water level in the effluent gas in pure Ar flow showing that water was removed from the gas stream, the temperature was decreased in steps to 35 °C and background spectra were recorded for each temperature. Then, 0.2 vol.% CO was introduced at 35 °C for 1 h, and the CO desorption was initiated by increasing the temperature in steps to 211 °C in Ar. Subsequently, CO oxidation was carried out by introducing 0.2 vol.% CO and 1 vol.% O_2 for 30 min and the temperature was decreased in steps to 35 °C. Each spectrum was acquired 10 min after reaching the set temperature using the corresponding background spectrum for each temperature.

2.3.2. X-ray absorption spectroscopy

The chemical state and coordination of Pt were studied by X-ray absorption spectroscopy at beamline P65 at PETRA III, Deutsches Elektronen-Synchrotron (DESY) in Hamburg, Germany. Spectra

for the Pt L_3 edge (11564 eV were measured in fluorescence mode with a passivated implanted planar silicon (PIPS) detector first *ex situ* for Pt black (Alfa Aesar) and PtO_2 (Alfa Aesar) references and then for Pt/alumina and Pt/ceria during CO oxidation. In the latter case, the current catalyst sample was filled in a quartz capillary reactor with an outer diameter of 1.5 mm, length of 80 mm and wall thickness of 0.01 mm. Spectra of the as-prepared catalysts were recorded in He at RT. Then the temperature was increased to 168 °C for Pt/alumina and 250 °C for Pt/ceria and feeds of 10 ml/min of 5% CO and 40 ml/min of 5% O_2 were introduced for 30 min. Subsequently, the temperature was decreased in steps to 37 °C. XAS spectra were processed by Athena [32] and the EXAFS region of the spectra was analysed by Artemis [33].

3. Results and discussion

Before discussing the *operando* spectroscopic measurements of the chemistry and dynamics of platinum species during the catalytic extinction, a description of the basic characteristics of the Pt/ceria and reference Pt/alumina catalysts and their catalytic behaviour is given, which facilitates comparisons with previous reports.

3.1. Catalyst physical characteristics

The physical characteristics of the prepared Pt/alumina and Pt/ceria catalysts are summarised in Table 1. The table shows the SSA, apparent size of support crystallites and Pt loading, dispersion and particle size. The SSA is 140 and 131 m^2/g_{cat} for the Pt/alumina and Pt/ceria catalyst, respectively. These values fall within the typical ranges for alumina and ceria supported catalysts [34]. The dominant contributions to the SSAs come from the microporous support materials, which present sufficiently large areas to enable high Pt dispersions. The crystallinity of the samples was measured with PXRD. Fig. 1 shows the resulting diffractograms together with reference patterns for γ-alumina (PDF 00–010-0425) and CeO_2 fluorite structure (PDF 00–004-0593). As can be seen, the diffractogram for Pt/alumina and Pt/ceria matches the reference pattern for γ-alumina and fluorite CeO_2, respectively. Using the Sherrer equation, the apparent crystallite sizes were calculated to be 6.0 nm for alumina and 8.0 nm for ceria. The support crystallite size can also be determined from the TEM images shown in Fig. 2. The presented images reveal crystallite sizes around 10 nm for the alumina and ceria support, respectively. In principle one could expect larger deviations as TEM results necessarily depend on selected analysis regions whereas PXRD results STEM from a larger sample volume. Also larger deviations could be expected because of the different probing modes of TEM and PXRD and the fact that the crystal planes are oriented in different directions due to the

Table 1

Summary of catalyst physical characteristics including specific surface area (N_2 physisorption), apparent size of support crystallites (PXRD), Pt loading (XRF), Pt specific surface area, dispersion and particle size (CO chemisorption) and Pt particle size (STEM) for 2 wt% Pt/alumina and 1 wt% Pt/ceria.

	2 wt.% Pt/alumina	1 wt.% Pt/ceria
Specific surface area, SSA/$m^2g_{cat}^{-1}$	140	131
Support crystallite size, $d_{support}$/nm	6.0	8.0
Pt loading/wt%	1.91	1.06
Specific Pt area/$m^2g_{cat}^{-1}$	2.65	1.92
Pt dispersion/%	56	73
Pt particle size, d_{Pt}[a]/nm	2.0	1.5
Pt particle size d_{Pt}[b]/nm	1.3 ± 0.4	1.0 ± 0.2

[a] CO chemisorption analysis.
[b] STEM analysis.
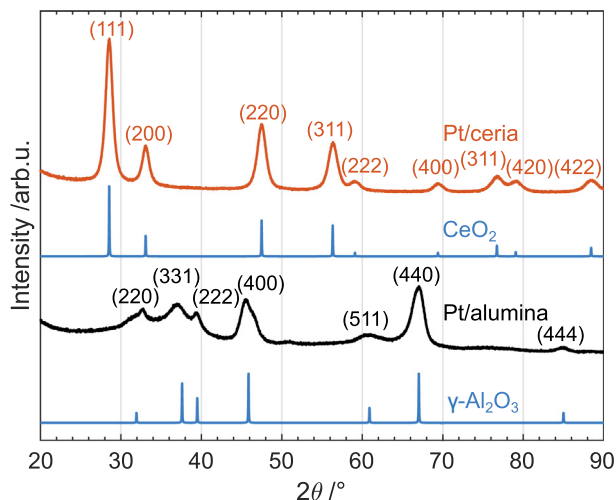
Fig. 1. XRD patterns of the Pt/ceria (orange) and Pt/alumina (black) catalysts. Reflection assignments are assigned using reference patterns (blue) from the Powder Diffraction File™ (PDF) database for CeO_2 (PDF 00–004-0593) and γ-Al_2O_3 (PDF 00–010-0425).

morphology, polycrystallinity and random orientation of the powder grains, which may be complicated by agglomeration. Further, the employed Scherrer equation is derived for the ideal situation with perfect materials crystallinity and no instrumental broadening, which is a simplification. Nevertheless, the support crystallite sizes obtained from TEM and PXRD are in good agreement.

Concerning the Pt phase, the diffractograms contain no visible peaks related to Pt. This is indicative of a majority of the Pt crystal-lites being amorphous and/or too small to give rise to clear diffraction, or diffracting crystallites are to few to produce detectable reflections [35,36]. Considering the Pt phase in more detail it is clear from the XRF and CO chemisorption measurements that because of the higher Pt loading for the Pt/alumina catalyst, the specific Pt area is higher, 2.65 m^2/g_{cat}, and the Pt dispersion is lower, 56%, as compared to the Pt/ceria catalyst for which the corresponding numbers are 1.92 m^2/g_{cat} and 73%, respectively. The higher Pt dispersion signifies not only smaller Pt particles, 2.0 nm for Pt/alumina and 1.5 nm for Pt/ceria, but likely also a narrower Pt particle size distribution [37]. This is in line with the interpretation that the Pt particles are too small to give clear reflections in the PXRD measurements. The existence of small Pt nanoparticles is evidenced also by electron microscopy measurements. Fig. 2 shows TEM (panel a and d) and STEM (panel b and e) images together with there from estimated Pt particle size distribution (PSD) for the Pt/alumina (panel c) and Pt/ceria (panel f) catalysts. Considering the Pt PSD for Pt/alumina, the majority of the particles appears to be in the range 0.7 to 1.5 nm with a mean Pt particle size of 1.29 nm. The Pt particles in the Pt/ceria catalyst are not as clearly presented in the TEM Fig. 2d. This is partly due to the small difference in mass between Pt and Ce, and partly due to a varying thickness of the specimen leading to a poor mass-thickness contrast. However, in the STEM image in Fig. 2e, Pt particles around 1 nm can be discerned thanks to the difference in Z number. The Pt/ceria catalyst contains numerous smaller Pt particles, as compared to Pt/alumina, with the majority of the particles in the narrow range of 0.5–1.3 nm and most particles are below 1.1 nm.

The (small) differences between estimated Pt particle size from CO chemisorption data and STEM imaging may have different explanations. Again, although not probable, the STEM imaging could be biased by a limited analysis region and/or number of
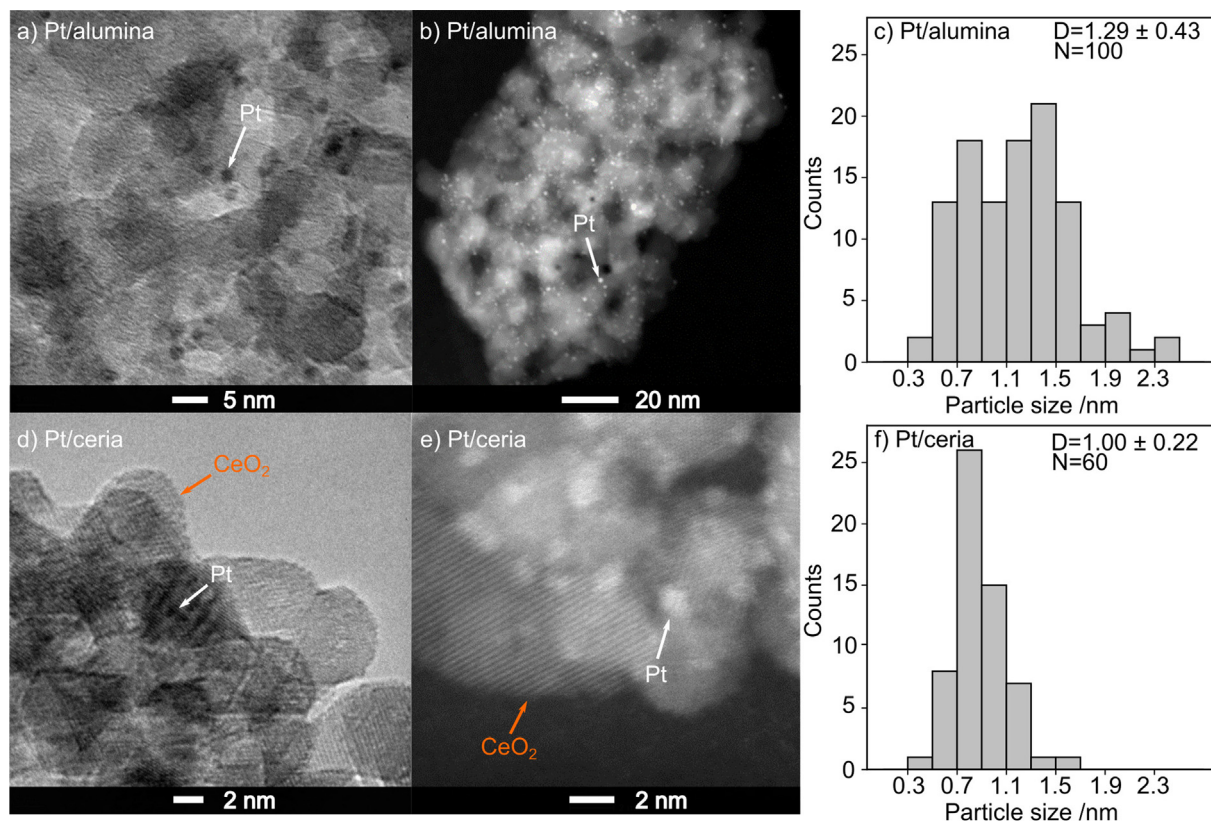
Fig. 2. High-resolution TEM and STEM-HAADF micrographs of the Pt/alumina (panel a and b) and Pt/ceria (panel d and e) catalysts. The Pt particle size distribution for Pt/alumina (panel c) shows an average size of 1.3 nm based on 100 Pt particles and for Pt/ceria (panel f) an average size of 1.0 nm based on 60 particles.

observable particles. Nevertheless, one would expect the estimated particle size from CO chemisorption data to be smaller than that of STEM imaging as all CO adsorption sites are probed whereas the smallest particles are not easily imaged. Small platinum particles, however, are significantly affected by the support, which could weaken the CO adsorption on some Pt sites leading to an overestimation of the Pt particle size. Despite this, the results from the different methods are in good agreement with each other. Finally, the STEM micrograph and EDX spectra in Supplementary Figure S1 reveal a Pt/Ce ratio of 0.36 and 0.41 for regions with visible Pt particles (position 1) and regions where no obvious Pt particles exist (position 2), respectively. Clearly, the presence of Pt could be detected for both positions. This suggests the presence of atomically dispersed Pt on the ceria. As such, the EDX analysis align well with the all results showing the presence of highly dispersed platinum. The lower Pt/Ce ratio at position 1 is a result of a thicker specimen in this area.

3.2. Catalytic extinction behaviour

The CO oxidation extinction profiles measured in the chemical flow-reactor are shown in Fig. 3a. The CO conversion for Pt/alumina (dashed line) and Pt/ceria (solid line) is clearly dependent on the CO concentration in the feed. The higher the feed CO concentration, the higher the extinction temperature, which is in line with previous studies [14,38]. The CO conversion for the Pt/alumina catalyst starts to drop at approximately 215, 190 and 150 °C when feeding 0.5, 0.2 and 0.05 vol% CO, respectively, whereas the corresponding temperatures for the Pt/ceria catalyst are 170, 160, and 135 °C. In terms of extinction temperatures, Pt/ceria is here shown to be more active for CO oxidation than Pt/alumina, especially considering its lower specific Pt area as has been observed previously [14,39]. As reflected by the narrower range of extinction temperatures, the dependence on the CO concentration in the feed is weaker for the ceria supported platinum. The qualitative kinetic behaviour of the Pt/alumina catalyst resembles that of Pt catalysts with inactive supports [40,41] and even that of unsupported Pt [42]. Upon decreasing the temperature, the competitive adsorption between CO and O_2 suddenly favours CO adsorption (first order kinetic phase transition) such that the Pt sites become CO self-poisoned and the CO oxidation rate drops [13,15].

Interestingly, for the Pt/ceria catalyst in the low CO conversion regime, the catalytic extinction slows down and the CO conversion decays slowly towards lower CO conversions in stark contrast to the Pt/alumina catalyst. The kinetic behaviour of the Pt/ceria catalyst at low CO conversions shows that Pt/ceria is less prone to CO

self-poisoning and suggests that complementary reaction paths that are less sensitive to CO poisoning [14,23] exist.

The different influence of alumina and ceria on Pt when used as support for Pt particles is further evidenced by the H_2-TPR measurements. Fig. 3 shows the H_2 consumption for Pt/alumina (panel b) and Pt/ceria (panel c) as a function of sample temperature together with a deconvolution of the main consumption peaks into Gaussian peaks. For the Pt/alumina, three peaks centred at 76, 212 and 379 °C could be fitted. Integration of the peak areas gives a H_2 consumption of 0.035, 0.08 and 0.2 mmol/g_{cat}, respectively. Different peaks are commonly assigned to Pt particles of different sizes [43]. According to the STEM imaging, however, the Pt particle size distribution is not broad. Thus, the three H_2 consumption peaks are assigned to different reduction processes. The low-temperature peak is presumably associated with surface reduction of oxidised Pt particles, likely the larger ones within the distribution, as well as platinum oxides weakly stabilised by the alumina support [44,45]. The peak at 212 °C is broad and not straightforward to assign to a certain species but merely reflects a continuous reduction with increasing temperature. The high-temperature peak is the major contributor to the overall H_2 consumption and almost represents the expected nominal H_2 consumption for complete reduction of PtO_2 to Pt. The high reduction temperature reflects reduction of platinum oxide particles that are significantly stabilised by the alumina support [46], supposedly the smaller ones within the distribution. As the H_2 consumption is close to the upper limit for a fully oxidised platinum phase, alternative consumption processes can be reflected upon. For example, it not imposible that H_2 is consumed by reactions with alumina bound surface carbonates. This effect, however, is likely minor as in the Pt/alumina system, the amount of carbonates remaining after pretreatment is expected to be too low [47]. Further, the use of 20 vol. % O_2 in the pretreatment is likely to result in a deep oxidation of the platinum phase such that close to nominal H_2 consumption during the TPR is not unrealistic.

The H_2 consumption profile for the Pt/ceria catalyst is apparently different from that of Pt/alumina. Here two peaks, both at rather low temperatures, could be fitted. The peak at 77 °C corresponds to the largest consumption amounting 0.4 mmol/g_{cat}. This peak is assigned to reduction of platinum oxides. However, the expected nominal H_2 consumption for reduction of Pt^{4+} to Pt in this sample is 0.1 mmol/g_{cat}. Thus, this peak reflects also other consumption routes. Presumably reactions between hydrogen and lattice oxygen in the vicinity of the Pt particle-ceria boundary [48] through hydrogen spillover [49,50] reducing Ce^{4+} cations adjacent to the Pt particles. Following this reasoning, the peak at 120 °C may be related to continued hydrogen migration requiring slightly
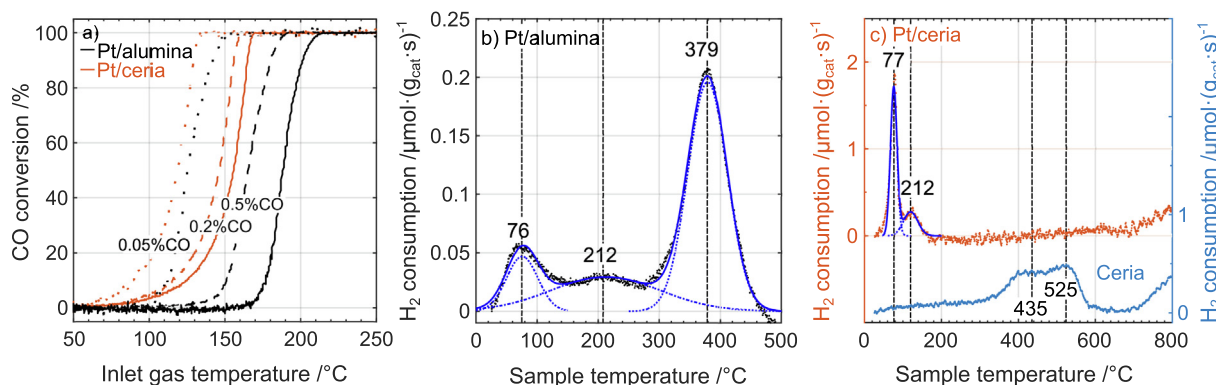

Fig. 3. Extinction profiles for CO oxidation (panel a) over Pt/alumina (black) and Pt/ceria (orange) under lean conditions with 0.5% (solid lines), 0.2% (dashed lines) and 0.05% CO (dotted lines) using 2% O_2. Deconvolution of H_2 reduction peaks after 20% O_2 pre-oxidised over Pt/alumina (panel b), ceria and Pt/ceria (panel c) at 250 °C is noted in dashed blue lines. The center of the individual deconvoluted peaks is marked and their sum is displayed with solid blue lines.

higher temperatures. For example it has been proposed that such migration can lead to the formation of ceria bronzes (H_xCeO_2) [9,50]. In Fig. 3c, the H_2 consumption by the ceria alone is included for comparison. As can be seen two reduction peaks appear at 435 and 525 °C, which previously have been assigned to surface reduction, whereas bulk reduction occurs at even higher temperature [9,39,51]. These peaks are absent for the Pt/ceria catalyst indicating that Pt is well distributed on the ceria surface in correspondence with the STEM/EDX results. Further, the absence of low-temperature peaks (at 77 and 120 °C) for ceria strengthens the interpretation that these originate from the Pt phase in the case of the Pt/ceria catalyst. The H_2-TPR results clearly show that the mechanisms mediated by the two supports are different. Hydrogen spillover and further reaction with oxygen from the support is significant for the Pt/ceria system whereas such processes seem negligible for Pt/alumina under the present conditions. This strengthens the interpretation that a platinum-ceria boundary can provide complementary CO oxidation reaction paths to those occurring on Pt particles.

3.3. Speciation and stability of CO ad-species

Carbon monoxide is one of the common probe molecules for catalytic sites and when combined with infrared spectroscopic characterisation, the resulting absorption bands from adsorbed CO signify sites with different coordination and chemistry [20,47,52,53]. Fig. 4 shows the IR spectra collected during desorption of pre-adsorbed CO upon a step-wise increase of the temperature. Princiaplly, the relative intensity of an IR band should not be interpreted as a relative abundance straight away as the molar attenuation coefficient depends on the configuration of the CO ad-species and the site it occupies. However, according to calculations (not shown), the variation of IR band intensity of platinum carbonyls of different configurations as well as platinum bound to oxygen is expected to be less than about threefold in most cases. Hence, (semi) quantitative comparison of IR bands in terms of ranking of species abundance can be made if the compared intensities differ more.
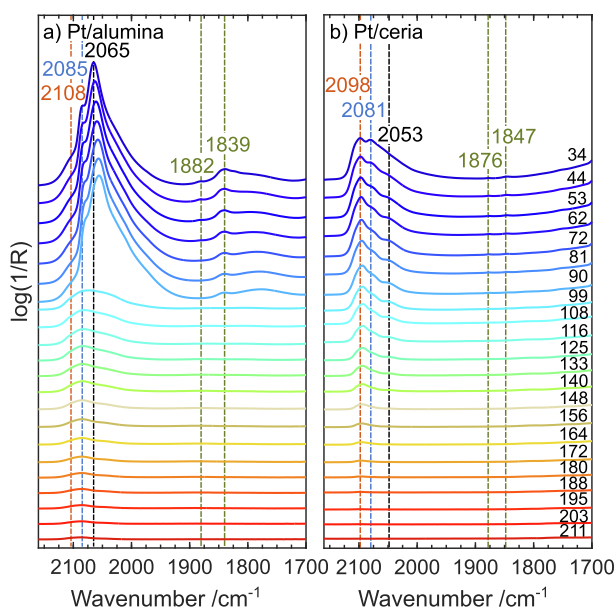
Fig. 4. Desorption of CO from Pt/alumina (a) and Pt/ceria (b) during a stepwise increase of the temperature from 34 to 211 °C. The catalysts were pretreated with 5% O_2 and then with 1% H_2 for 30 min at 211 °C, cooled and exposed to 0.2% CO at 34 °C until saturation.

Three major peaks positioned at 2108, 2085 and 2065 cm^{-1} can be seen for the Pt/alumina catalyst (panel a). These are assigned to CO linearly bonded to ionic platinum ($\tilde{v}_{lin}^{CO}(Pt^{2+})$), partially oxidised platinum ($\tilde{v}_{lin}^{CO}(Pt^{\delta+})$) and reduced platinum ($\tilde{v}_{lin}^{CO}(Pt^0)$), respectively [52,54–56]. The two minor peaks at 1882 and 1839 cm^{-1} are assigned to CO bridge-bonded to platinum ($\tilde{v}_{br}^{CO}(Pt)$) likely on larger Pt particles [20,57]. A comparison of the peak intensities suggests that the vast majority of the adsorbed CO species is of linear configuration as the $\tilde{v}_{lin}^{CO}$ is at least 15 times more intense than the $\tilde{v}_{br}^{CO}$. This supports the assumption of a one-to-one relationship between adsorbed CO and number of Pt surface atoms used in the analysis of CO chemisorption data above. Upon increasing the temperature, adsorbed CO starts to desorb as evidenced by the generally decreasing intensity over the entire measured spectral range. For temperatures up to 90 °C, the $\tilde{v}_{lin}^{CO}(Pt^0)$ band can be clearly seen and it red-shifts by 9 cm^{-1}. This can be explained by two effects, i.e., a successively weaker CO dipole–dipole coupling and increasing back donation of electrons to the $2\pi^*$ molecular orbital in the adsorbed CO with decreasing CO coverage [58]. Increasing the temperature further leads to an abrupt change in the entire spectrum at 99 °C. At this temperature the peaks for $\tilde{v}_{lin}^{CO}(Pt^{2+})$, $\tilde{v}_{lin}^{CO}(Pt^{\delta+})$ and $\tilde{v}_{lin}^{CO}(Pt^0)$ can be seen, but the $\tilde{v}_{lin}^{CO}(Pt^{\delta+})$ peak becomes the dominant species. Likely, this peak reflects CO ad-species on Pt sites that connect with the alumina support, giving rise to the partially oxidised character of the Pt site.

Moving on to the Pt/ceria catalyst, peaks at 2098, 2081 and 2053 cm^{-1} are assigned to $\tilde{v}_{lin}^{CO}(Pt^{2+})$, $\tilde{v}_{lin}^{CO}(Pt^{\delta+})$ and $\tilde{v}_{lin}^{CO}(Pt^0)$, respectively [59,60]. It is clear that the majority of the CO ad-species bind to oxidised platinum demonstrating the significant impact of the ceria support on these platinum sites. There are also some (minor) CO adsorbed on Pt^0 indicating the presence of Pt particles exposing sites that are not significantly affected by the ceria support. In addition to the $\tilde{v}_{lin}^{CO}$ bands there are two minor peaks at 1876 and 1847 cm^{-1} that can be assigned to $\tilde{v}_{br}^{CO}(Pt)$ [61]. Following the same reasoning as for the Pt/alumina system, the $\tilde{v}_{lin}^{CO}$ is the most abundant species and the assumption of a one-to-one ratio for adsorbed CO and Pt sites is valid also for the Pt/ceria system. Upon increasing the temperature, CO starts to desorb. The $\tilde{v}_{br}^{CO}$ bands disappear first and cannot be discerned when reaching 116 °C whereas the $\tilde{v}_{lin}^{CO}(Pt^0)$ band has vanished at roughly 172 °C. The $\tilde{v}_{lin}^{CO}(Pt^{\delta+})$ and $\tilde{v}_{lin}^{CO}(Pt^{2+})$ band can be seen for temperatures up to around 180 °C and 188 °C, respectively. Interestingly, no obvious red-shift is unveiled as for the Pt/alumina catalyst. This indicates that the Pt particles are too small and/or curved as to provide surfaces for which coverage dependent peak shifts could occur. Another explanation, also stemming from the small particle size, is that the characteristics of the majority Pt sites is dominated by their interactions with support oxygen. A less likely explanation could be that charge transfer from Pt to cerium atoms [62] impose a blue-shift that perfectly compensates a coverage-dependent red-shift [61].

Comparing the type and stability of the CO ad-species for the Pt/alumina and Pt/ceria catalysts, it is found that the most abundant species is the $\tilde{v}_{lin}^{CO}$ for both samples. However, at low temperatures, the main characteristic peak for Pt/alumina is the $\tilde{v}_{lin}^{CO}(Pt^0)$ whereas for Pt/ceria it is the $\tilde{v}_{lin}^{CO}(Pt^{2+})$, clearly showing that the support influences the chemical properties of many Pt sites. For both catalysts, CO adsorbed on Pt with oxidised character appears most stable. Specifically, the most stable ad-species for the Pt/alumina and Pt/ceria catalysts is $\tilde{v}_{lin}^{CO}(Pt^{\delta+})$ and the $\tilde{v}_{lin}^{CO}(Pt^{2+})$, respectively. This is a result of the interaction between the support and the generally small particles as CO binds significantly weaker on a true platinum oxide particle than on the corresponding metallic platinum particle [20]. The IR bands for the Pt/ceria catalyst are gener-

ally less intense. One cannot unambiguously state whether or not this stems from fewer CO ad-species because the molar attenuation coefficients for the CO ad-species could be different for the ceria system. Further, other optical properties, foremost scattering, of ceria is likely different from that of alumina, ultimately leading to varying optical path length in the sample bed. This inherent property cannot be eliminated but the use of a thin layer of sample on top of a KBr bed as to probe the full sample depth may at least counteract this artefact. Hence, one can only speculate that the lower intensity reflects fewer adsorbates, which then suggests that parts of the platinum interacts weakly with CO. Supposedly such platinum species is atomically dispersed platinum [63], which aligns well with the fact that the Pt is more dispersed on the ceria support. The more dispersed platinum may also explain the positions of the characteristic IR peaks that appear at lower wavenumbers as compared to the Pt/alumina catalyst. These positions may relate to the smaller size and possibly different morphology of the Pt particles and/or overall less dense CO coverage.

3.4. Chemistry and dynamics of Pt particles during catalytic extinction

Turning to the main question, namely how the support influences the chemistry of the Pt particles during catalytic extinction, *operando* DRIFTS and XAS were used and correlated as presented for Pt/alumina in Fig. 5 and for Pt/ceria in Fig. 6. In these figures, the a panels show the spectral region for $\tilde{v}_{gas}^{CO_2}$ formed as a direct consequence of the catalytic reaction together with CO conversions measured with mass spectrometry, the b panels the wavenumber region for the different CO ad-species on Pt analogous to the CO desorption discussed above, the c panels the normalised XANES spectra and d panels the fitted k^2-weighted EXAFS spectra. As-prepared samples, Pt black and PtO_2 are used as as references for the XAS measurements. The percentage of CO conversion measured by mass spectrometry is shown on the FT k^2-weighted EXAFS spectra.

Starting with the results for the reference Pt/alumina catalyst, it is clear that at the highest temperature of 211 °C, the $\tilde{v}_{gas}^{CO_2}$ band has maximum intensity whereas no bands for CO ad-species can be observed. This reflects a highly active catalyst free from CO poisoning. With decreasing temperature, the intensity of the $\tilde{v}_{gas}^{CO_2}$ band decreases, at first, rather continuously until 116 °C is reached from where it drops. This drastic change in CO_2 production is associated with a corresponding abrupt change in the intensities for the $\tilde{v}_{lin}^{CO}$. At 108 °C, the $\tilde{v}_{gas}^{CO_2}$ band is almost vanished and the $\tilde{v}_{lin}^{CO}$ bands grow even stronger. Qualitatively this is in line with the flow-reactor results. Upon decreasing the temperature, the activity for CO oxidation declines and at the critical temperature, here around 108 °C, the kinetics changes drastically when the Pt sites become CO self-poisoned (kinetic phase transition). The $\tilde{v}_{lin}^{CO}$ bands, however, start to be visible already at 133 °C when some CO_2 is produced. This is likely due to the presence of Pt particles with different sizes exposing Pt sites with different activity. For technical catalysts, this is an important characteristics as to be functioning in a broad temperature interval. The $\tilde{v}_{br}^{CO}$ bands are not visible until the CO_2 production ceases at 108 °C from where they grow stronger during the further decrease of the temperature. Compared to the CO desorption measurements, the $\tilde{v}_{lin}^{CO}(Pt^{2+})$, $\tilde{v}_{lin}^{CO}(Pt^{\delta+})$ and $\tilde{v}_{lin}^{CO}(Pt^0)$ bands are generally positioned at higher wavenumbers, i.e., 2112, 2090 and 2069 cm^{-1}, respectively. On the contrary, the $\tilde{v}_{br}^{CO}$ bands appear at nearly the same positions. The higher wavenumbers for the $\tilde{v}_{lin}^{CO}$ bands reflect that CO adsorbs linearly on Pt sites that are affected by the presence of oxygen whereas the sites adsorbing CO in bridged configuration seem unaffected. During the extinction, when the CO self-poisoning occurs, the oxi-
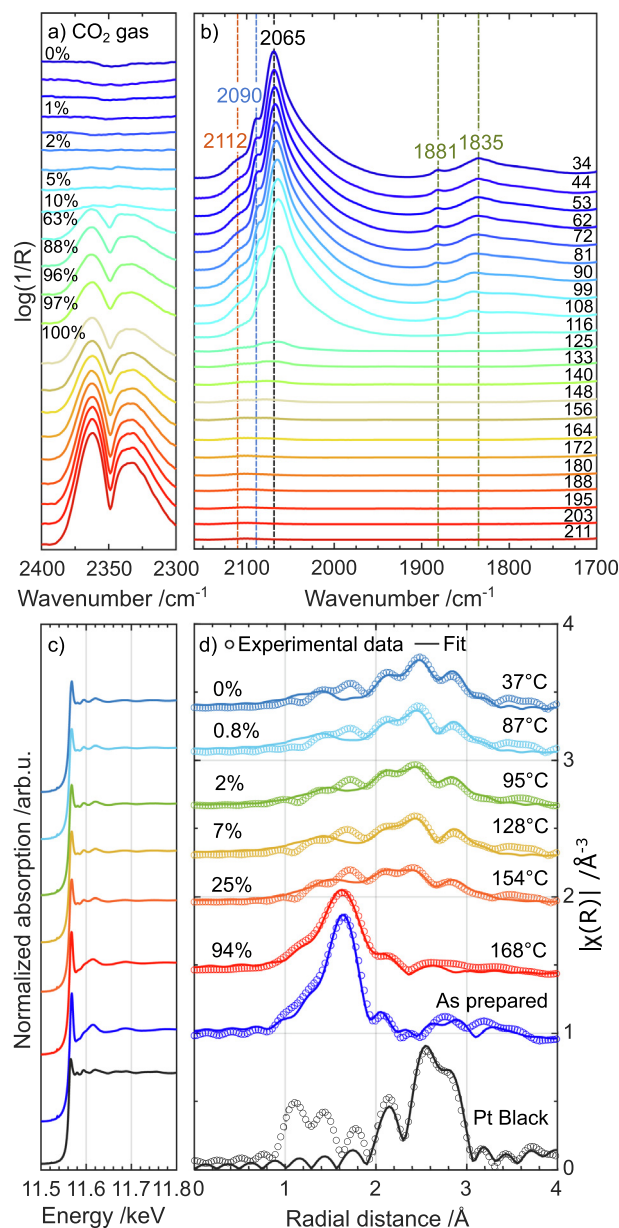
Fig. 5. *Operando* spectroscopic results for Pt/alumina during catalytic CO oxidation extinction. CO_2 gas phase spectra with noted CO conversions measured with mass spectrometry (panel a) and spectral region for CO adsorbed on Pt (panel b) with noted sample temperatures in °C in presence of 0.2 vol.% CO and 1 vol.% O_2. XANES spectra (panel c) and FT k^2-weighted EXAFS spectra with noted CO conversions (panel d) in a flow of 10 ml/min of 5 vol.% CO and 40 ml/min of 5 vol.% O_2. The spectrum for Pt black (panel d) was recorded *ex situ* in ambient air at room temperature as a reference.

dised parts of Pt particles are expected to undergo reduction [22] that leads to a red-shift of the $\tilde{v}_{lin}^{CO}(Pt^0)$ band [20]. This may be discerned at the very beginning of the build-up of the $\tilde{v}_{lin}^{CO}(Pt^0)$ band although not very clearly. Likely, this red-shift is cancelled out by the blue-shift caused by increasing CO coverage. As bridge-bonded CO can be observed only after the catalytic extinction, the removal of platinum oxides is likely close to complete at this point resulting in unaltered band positions. Looking at the evolution of the Pt L_3 edge, it is clear that the white-line intensity decreases (step-wise) during the extinction, here between 168 and 154 °C. Likewise, the FT k^2-weighted EXAFS spectra show a clear peak at 1.5–2 Å assigned to Pt—O contribution at the higher
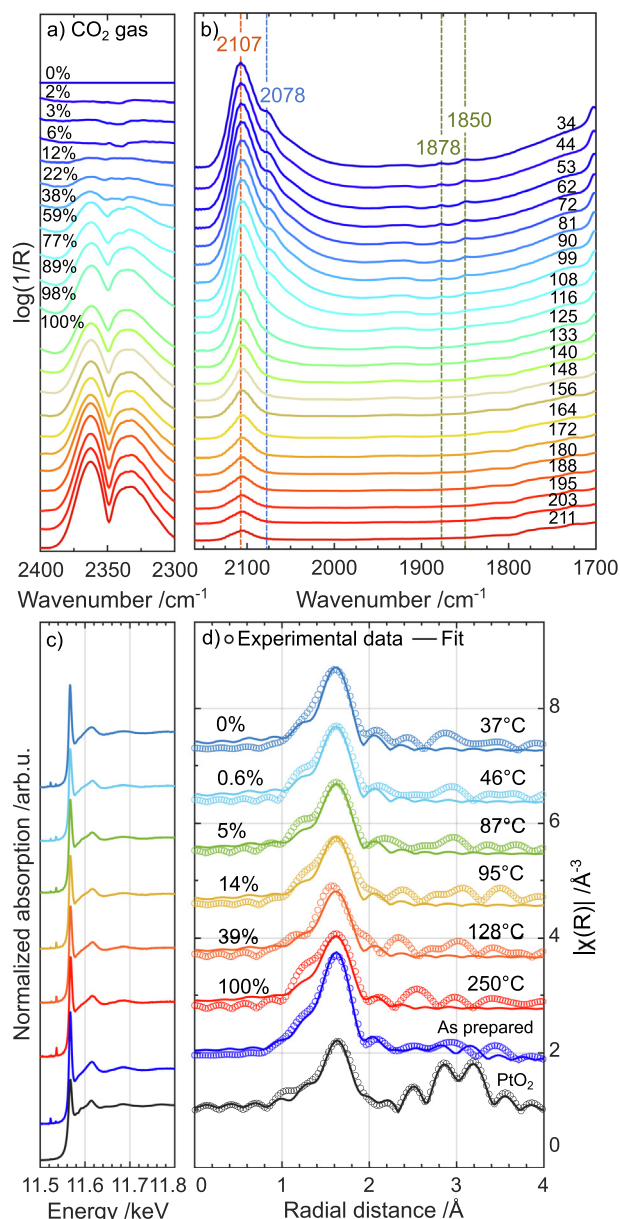
Fig. 6. *Operando* spectroscopic results for Pt/ceria during catalytic CO oxidation extinction. CO_2 gas phase spectra with noted CO conversions measured with mass spectrometry (panel a) and spectral region for CO adsorbed on Pt (panel b) with noted sample temperatures in °C in presence of 0.2 vol.% CO and 1 vol.% O_2. XANES spectra (panel c) and FT k^2-weighted EXAFS spectra with noted CO conversions (panel d) in a flow of 10 ml/min of 5 vol.% CO and 40 ml/min of 5 vol.% O_2. Reference spectra for PtO_2 and Pt foil were recorded *ex situ* in ambient air at room temperature.

temperature when the CO oxidation proceeds whereas during extinction, a pronounced peak at around 2.5–3 Å assigned to Pt—Pt contribution appears at the expense of Pt—O contribution. The DRIFTS and XAS data together reflect that the oxidised state of Pt during CO oxidation is caused by O_2 dissociation on Pt particles and during the catalytic extinction, CO adsorbs preferentially on Pt sites leading to a reduction of platinum oxides and a CO self-poisoned catalyst. In essence the CO oxidation is in line with the classical three-step mechanism complemented with oxide formation [13,20]. However, some of the Pt sites, likely those on the smaller Pt particles, exhibit a certain oxidised character due to the presence of oxygen even at low CO conversions.

Moving to the oxidation of CO over the Pt/ceria catalyst, the measured spectroscopic response during catalytic extinction (cf. Fig. 6) is qualitatively different from that of Pt/alumina. Even at the highest temperature of 211 °C, at which the measured CO_2 product is obviously significant and CO conversion is 100%, an IR absorption band at 2107 cm^{-1} with a fwhm of 20–30 cm^{-1} can be clearly seen. This band is assigned to CO linearly bonded to ionic platinum, i.e., $\tilde{v}_{lin}^{CO}(Pt^{2+})$. This species appears to be a spectator that seems to be in equilibrium with gas phase CO as its band intensity increases with decreasing temperature while the CO conversion remains complete. It is not trivial to elucidate its origin and reported IR band assignments are not free from debate [27]. Here, the peak is neither observed for Pt/alumina nor Pt/ceria during CO-TPD conditions, i.e., no CO in the feed, suggesting the bonding of CO to the site is not strong and/or that the site is not present without oxygen in the feed. From a catalysis point of view, one may speculate that it signifies CO adsorbed on atomically dispersed platinum that has been considered catalytically inactive. However, such species has been reported to give rise to a sharp IR band at 2090 cm^{-1} with fwhm around 10 cm^{-1}. For example for single atom catalysts prepared by a sol–gel method [24] and catalysts with platinum substituted into ceria admittedly prepared with incipient impregnation but with post-calcination reductive treatment [64]. On the contrary, for catalysts synthesised with strong electrostatic adsorption and incipient wetness impregnation methods that provide a more relevant comparison with present samples, the CO adsorption on atomically dispersed platinum has been shown to be weak [63]. Instead, the observed IR band at 2095 cm^{-1} has been assigned to CO on oxidised platinum clusters [63]. Further, CO adsorption on presumably rather deeply oxidised platinum particles on alumina has been associated with IR bands at 2112 cm^{-1} [20], which is close to present peak position. Taken together, the present spectroscopic data points towards a $\tilde{v}_{lin}^{CO}(Pt^{2+})$ species originating from oxidised platinum clusters and/or PtO_x patches on particles, which suggests coexisting platinum and platinum oxide phases. Such phases have been considered to synergistically drive the CO oxidation reaction where the platinum phase adsorbs the CO and the oxide phase provides reactive O [65]. The present results are in line with this mechanism although the presence of catalytically inactive platinum oxides, which cannot be reduced by CO under present reaction conditions, can not be excluded. Considering the latter to be clusters, one may envisage (planar) moeties in close contact with the ceria support that exist only under oxidising atmosphere maintaining the clusters and/or ceria oxidised.

Upon decreasing the temperature, the intensity of the $\tilde{v}_{gas}^{CO_2}$ band decreases smoothly without a drastic change. Simultaneously, the $\tilde{v}_{lin}^{CO}(Pt^{2+})$ immediately starts to grow despite continued formation of CO_2. Reaching 125 °C, less CO_2 is formed and at 81 °C it is hardly visible. At around 125 °C, a shoulder at 2078 cm^{-1} assigned to $\tilde{v}_{lin}^{CO}(Pt^{\delta+})$ starts to evolve. The appearance of this shoulder reflects removal of platinum-bound oxygen by CO during the extinction. As the $\tilde{v}_{lin}^{CO}(Pt^{\delta+})$ band appears as a shoulder, this type of site likely constitutes a smaller part of the total number of available Pt sites, in line with a previous study [47]. This extinction dynamics indicates that the CO oxidation in the high reactive state proceeds on partially oxidised platinum particles suggesting that the reaction uses CO adsorbed on Pt and O from PtO_x species similar to previous works [22,65].

Scrutinising the XANES spectra, there is hardly any visible changes in the Pt L_3 edge intensity during the extinction. Considering the EXAFS spectra, the Pt phase remains in an oxidised state with a clear Pt—O contribution and negligible Pt—Pt coordination during the entire extinction process. It appears oxidised even at 37 °C when the reaction is extinct. In fact, during reaction condi-
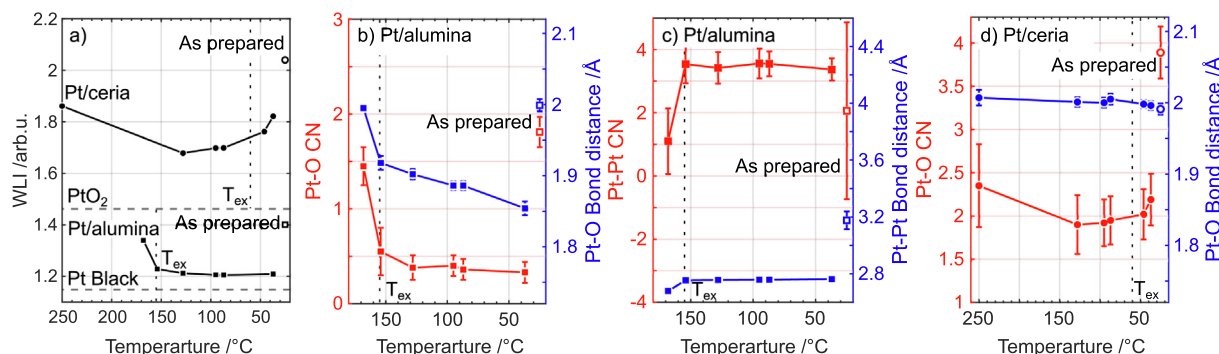
Fig. 7. Temperature variation of the whiteline intensity (WLI) for Pt/alumina and Pt/ceria (panel a), coordination number (CN) and radial distance (R) without phase correction for Pt—O and Pt—Pt scattering of Pt/alumina (panel b and c) and Pt/ceria (panel d).

tions the oxidation state is only slightly lower than for the as-prepared Pt/ceria under He flow at RT, and Pt clearly coordinates with O. This is, again, explained by the highly dispersed platinum, i.e., the presence of small Pt particles and atomically dispersed Pt, that make the majority of the included Pt atoms to bind to support oxygen.

To further analyse the oxidation state of Pt, the so-called whiteline intensity (WLI) is plotted as a function of temperature for the two samples in Fig. 7a. For Pt/alumina the WLI is always between that of Pt black and PtO_2. For the as-prepared Pt/alumina the WLI is rather close to that of PtO_2 whereas in the presence of the reaction mixture the maximum WLI observed for the active catalyst is slightly lower and drops during extinction. The lowest value, however, obtained for the CO self-poisoned catalyst is still higher than that for Pt black, which indicates a certain (small) influence by the alumina support on the Pt particles assuming complete oxide removal by CO. For the Pt/ceria catalyst, the WLI is generally considerably higher and the changes during catalytic extinction are different from those of Pt/alumina. The WLI first decreases from 1.85 to 1.7 where it remains until the catalytic extinction occurs and then increases. This behaviour is not straightforward to explain. One can, however, envisage that CO reacts with lattice oxygen from ceria support in the vicinity of Pt particles resulting in a slight decrease of the WLI in the high temperature regime and then, when the reaction extincts, formed oxygen vacancies in the ceria support become replenished by O_2 at low temperatures [66]. This interpretation implies a clear interplay between ceria and Pt particles and specifically that reactions at the platinum-ceria boundary is possible at low temperatures.

The different impact of the two supports on the Pt particles becomes even clearer when analysing the local structure. The coordination number (CN) and bond distance for Pt—O and Pt—Pt species are plotted as a function of temperature for the two samples in Fig. 7b-d. The fitting parameters for Pt/alumina and Pt/ceria are shown in Supplementary Table S2 and Supplementary Table S1, respectively. For the Pt/alumina catalyst, the Pt—O CN generally follows the same trend as the WLI. In the presence of the reaction mixture, a high Pt—O CN is observed only at 168 °C, for which the catalytic activity is high. The Pt—O bond distance is equivalent to the as-prepared sample and slightly shorter than that of PtO_2 suggesting a deformed platinum oxide as proposed earlier [22]. For the lower temperatures with low catalytic activity the Pt—O CN is also low. Here, instead, the Pt—Pt CN is generally high except at 168 °C and increases during the extinction process indicating an increasing presence of Pt particles that have been reduced by CO. At low temperatures, the Pt—Pt bond distance is lower than for the as-prepared sample but close to that of Pt black. For Pt/ceria, during CO oxidation, the Pt—O CN follows the same trend as the WLI, i.e., first a decrease to a minimum level where it stays until the cat-

alytic extinction occurs and then increases again. This indicates that the major contribution to the observed changes in WLI originates from Pt—O species. The high oxidation state of Pt when supported on ceria is most likely due to its binding to ceria lattice oxygen creating stable Pt—O structures, for example, the Pt—O distance of about 2 Å remains nearly unchanged in agreement with other studies on platinum nanoparticles on nanosized ceria [67]. The marginally longer Pt—O distance at elevated temperature is due to thermal expansion. Further, the platinum oxidation state is influenced by charge transfer from the Pt particles to cerium [68,69]. Despite being a bulk averaging technique, the XAS measurements include these effects because of the high Pt dispersion. It has been proposed that electrons from Pt nanoparticles can transfer to (nanosized) ceria when supplemented with ceria lattice oxygen spillover to the vicinity of Pt [48,70].

In summary the two support materials influence the chemistry and dynamics of the Pt particles differently leading to qualitatively different extinction behaviour for CO oxidation. Under CO oxidation conditions, platinum particles on both alumina and ceria are in an oxidised state. For Pt/alumina, the extinction of the CO oxidation occurs with a drop in catalytic activity caused by a sudden build up of the CO coverage, which is associated with removal of platinum oxides such that the state of Pt is close to that of Pt black experiencing just a minor influence by the alumina. Contrary, for Pt/ceria, the high oxidation state of Pt prevails during the extinction process, which is smooth rather than stepwise. Judging from the XAS results alone one would falsely claim that the Pt/ceria catalyst is active at all temperatures because of the high oxidation state suggesting no CO self-poisoning. With the infrared spectroscopic results, however, it is clear that at low temperatures also the Pt/ceria system is covered with CO. This emphasises the importance of correlative *operando* measurements in heterogeneous catalysis research.

4. Conclusions

Correlative *operando* infrared and X-ray absorption spectroscopy has been shown to be required as to explain the qualitatively different extinction kinetics of CO oxidation over industrially relevant Pt/ceria in comparison with reference Pt/alumina. Small Pt particles, with sizes centred around 1 nm, remain in a highly oxidised state independent of CO coverage and oxidation activity, which is suggested to be caused by their interaction with oxygens in the ceria lattice, possibly accompanied by charge transfer from platinum to cerium atoms. At high conversions, spectator CO adspecies can be observed while the reaction proceeds on platinum particles that contain ionic platinum. Despite a high CO coverage at low temperatures, some CO oxidation activity is observed suggesting accessible catalytic reaction pathways at the platinum-

ceria boundary that cannot be CO self-poisoned. Hence, the protracted extinction is explained by a gradual CO self-poisoning of sites on the platinum particles that shifts the main oxidation route from occurring on the particles, exposing Pt and PtO_x sites, to be mediated by sites at the platinum-ceria boundary. Approaching room temperature, these boundary sites eventually become inactive as well. This behavior is in stark contrast to that of Pt/alumina, which follows the classical extinction behavior with a reduction of PtO_x species and a drop in catalytic activity caused by a sudden CO self-poisoning, i.e., a first order kinetic phase transition.

CRediT authorship contribution statement

Mengqiao Di: Conceptualization, Investigation, Writing – original draft. **Kerry Simmance:** Investigation. **Andreas Schaefer:** Investigation, Writing – review & editing. **Yanyue Feng:** Investigation. **Felix Hemmingsson:** Investigation, Writing – review & editing. **Magnus Skoglundh:** Supervision, Writing – review & editing, Funding acquisition. **Tamsin Bell:** Writing – review & editing. **David Thompsett:** Supervision, Writing – review & editing, Funding acquisition. **Lucy Idowu Ajakaiye Jensen:** Investigation. **Sara Blomberg:** Investigation. **Per-Anders Carlsson:** Conceptualization, Supervision, Writing – review & editing, Funding acquisition.

Declaration of Competing Interest

The authors declare that they have no known competing financial interests or personal relationships that could have appeared to influence the work reported in this paper.

Acknowledgements

Appendix A. Supplementary material

Supplementary data associated with this article can be found, in the online version, at https://doi.org/10.1016/j.jcat.2022.03.022.

References

[1] C.G. Freyschlag, R.J. Madix, Precious metal magic: catalytic wizardry, Mater. Today 14 (2011) 134–142.
[2] W. Yu, M.D. Porosoff, J.G. Chen, Review of Pt-based bimetallic catalysis: From model surfaces to supported catalysts, Chem. Rev. 112 (2012) 5780–5817.
[3] A.I. Boronin, E.M. Slavinskaya, A. Figueroba, A.I. Stadnichenko, T.Y. Kardash, O. A. Stonkus, E.A. Fedorova, V.V. Muravev, V.A. Svetlichnyi, A. Bruix, K.M. Neyman, CO oxidation activity of Pt/CeO2 catalysts below 0 °C: platinum loading effects, Appl. Catal., B 286 (2021) 119931.
[4] J. Lee, J.R. Theis, E.A. Kyriakidou, Vehicle emissions trapping materials: Successes, challenges, and the path forward, Appl. Catal., B 243 (2019) 397–414.
[5] R.J. Farrauto, M. Deeba, S. Alerasool, Gasoline automobile catalysis and its historical journey to cleaner air, Nat. Catal. 2 (2019) 603–613.
[6] G. Ertl, H. Knözinger, J. Weitkamp, Handbook of Heterogeneous Catalysis, John Wiley & Sons Ltd, 2008.
[7] A.T. Bell, The impact of nanoscience on heterogeneous catalysis, Science 299 (2003) 1688–1691.
[8] H.S. Gandhi, G.W. Graham, R.W. Mccabe, Automotive exhaust catalysis, J. Catal. 216 (2003) 433–442.
[9] A. Trovarelli, Catalytic properties of ceria and CeO2-containing materials, Catal. Rev.: Sci. Eng. 38 (1996) 439–520.
[10] F.C. Meunier, D. Tibiletti, A. Goguet, D. Reid, R. Burch, On the reactivity of carbonate species on a Pt/CeO2 catalyst under various reaction atmospheres: Application of the isotopic exchange technique, Appl. Catal., A 289 (2005) 104–112.
[11] A. Bruix, J.A. Rodriguez, P.J. Ramírez, S.D. Senanayake, J. Evans, J.B. Park, D. Stacchiola, P. Liu, J. Hrbek, F. Illas, A new type of strong metal-support interaction and the production of H2 through the transformation of water on Pt/CeO2(111) and Pt/CeOx/TiO2(110) catalysts, J. Am. Chem. Soc. 134 (2012) 8968–8974.
[12] P.-A. Carlsson, M. Skoglundh, P. Thormählen, B. Andersson, Low-temperature CO oxidation over a Pt/Al2O3 monolith catalyst investigated by step-response experiments and simulations, Top. Catal. 30 (2004) 375–381.
[13] P.-A. Carlsson, V.P. Zhdanov, B. Kasemo, Bistable mean-field kinetics of CO oxidation on Pt with oxide formation, Appl. Surf. Sci. 239 (2005) 424–431.
[14] P.-A. Carlsson, M. Skoglundh, Low-temperature oxidation of carbon monoxide and methane over alumina and ceria supported platinum catalysts, Appl. Catal., B 101 (2011) 669–675.
[15] V.P. Zhdanov, B. Kasemo, Kinetic phase transitions in simple reactions on solid surfaces, Surf. Sci. Rep. 20 (1994) 113–189.
[16] P.-A. Carlsson, P. Thormählen, M. Skoglundh, H. Persson, E. Fridell, E. Jobson, B. Andersson, Periodic control for improved low-temperature catalytic activity, Top. Catal. 16 (2001) 343–347.
[17] P.-A. Carlsson, M. Skoglundh, E. Fridell, E. Jobson, B. Andersson, Induced low temperature catalytic ignition by transient changes in the gas composition, Catal. Today 73 (2002) 307–313.
[18] M. Kinne, T. Fuhrmann, J.F. Zhu, C.M. Whelan, R. Denecke, H.P. Steinrück, Kinetics of the CO oxidation reaction on Pt(111) studied by in situ high-resolution X-ray photoelectron spectroscopy, J. Chem. Phys. 120 (2004) 7113–7122.
[19] J. Wintterlin, S. Völkening, T.V. Janssens, T. Zambelli, G. Ertl, Atomic and macroscopic reaction rates of a surface-catalyzed reaction, Science 278 (1997) 1931–1934.
[20] P.-A. Carlsson, L. Österlund, P. Thormählen, A. Palmqvist, E. Fridell, J. Jansson, M. Skoglundh, A transient in situ FTIR and XANES study of CO oxidation over Pt/Al2O3 catalysts, J. Catal. 226 (2004) 422–434.
[21] P.-A. Carlsson, V.P. Zhdanov, M. Skoglundh, Self-sustained kinetic oscillations in CO oxidation over silica-supported Pt, Phys. Chem. Chem. Phys. 8 (2006) 2703–2706.
[22] E. Alayon, J. Singh, M. Nachtegaal, M. Harfouche, J.A. van Bokhoven, On highly active partially oxidized platinum in carbon monoxide oxidation over supported platinum catalysts, J. Catal. 263 (2009) 228–238.
[23] A.M. Gänzler, M. Casapu, D.E. Doronkin, F. Maurer, P. Lott, P. Glatzel, M. Votsmeier, O. Deutschmann, J.D. Grunwaldt, Unravelling the different reaction pathways for low temperature CO oxidation on Pt/CeO2 and Pt/Al2O3 by spatially resolved structure-activity correlations, J. Phys. Chem. Letters 10 (2019) 7698–7705.
[24] M. Kottwitz, Y. Li, R.M. Palomino, Z. Liu, G. Wang, Q. Wu, J. Huang, J. Timoshenko, S.D. Senanayake, M. Balasubramanian, D. Lu, R.G. Nuzzo, A.I. Frenkel, Local structure and electronic state of atomically dispersed Pt supported on nanosized CeO2, ACS Catal. 9 (2019) 8738–8748.
[25] Y. Lu, S. Zhou, C.T. Kuo, D. Kunwar, C. Thompson, A.S. Hoffman, A. Boubnov, S. Lin, A.K. Datye, H. Guo, A.M. Karim, Unraveling the intermediate reaction complexes and critical role of support-derived oxygen atoms in CO oxidation on single-atom Pt/CeO2, ACS Catal. 11 (2021) 8701–8715.
[26] H. Wang, J.-X. Liu, L.F. Allard, S. Lee, J. Liu, H. Li, J. Wang, J. Wang, S.H. Oh, W. Li, M. Flytzani-Stephanopoulos, M. Shen, B.R. Goldsmith, M. Yang, Surpassing the single-atom catalytic activity limit through paired Pt-O-Pt ensemble built from isolated Pt1 atoms, Nat. Commun. 10 (2019) 1–12.
[27] F.C. Meunier, Relevance of IR spectroscopy of adsorbed CO for the characterization of heterogeneous catalysts containing isolated atoms, J. Phys. Chem. C 125 (2021) 21810–21823.
[28] A.M. Gänzler, M. Casapu, F. Maurer, H. Störmer, D. Gerthsen, G. Ferré, P. Vernoux, B. Bornmann, R. Frahm, V. Murzin, M. Nachtegaal, M. Votsmeier, J.-D. Grunwaldt, Tuning the Pt/CeO2 interface by in situ variation of the Pt particle size, ACS Catal. 8 (2018) 4800–4811.
[29] A.M. Gänzler, M. Casapu, P. Vernoux, S. Loridant, F.J. Cadete Santos Aires, T. Epicier, B. Betz, R. Hoyer, J.D. Grunwaldt, Tuning the structure of platinum particles on ceria in situ for enhancing the catalytic performance of exhaust gas catalysts, Angew. Chem. Int. Ed. 56 (2017) 13078–13082.
[30] P. Gruene, A. Fielicke, G. Meijer, D.M. Rayner, The adsorption of CO on group 10 (Ni, Pd, Pt) transition-metal clusters, Phys. Chem. Chem. Phys. 10 (2008) 6144–6149.
[31] Rasband WS., ImageJ, 2021–06-04. https://imagej.nih.gov/ij/.
[32] Bruce Ravel, Athena: XAS data processing, 2009-2016. URL http://bruceravel. github.io/demeter/documents/Athena/index.html.
[33] Bruce Ravel 2009-2016, Artemis: EXAFS data analysis using feff with larch or ifeffit, 2009-2016. URL https://bruceravel.github.io/demeter/documents/ Artemis/index.html#artemis-exafs-data-analysis-using-feff-with-larch-or-ifeffit.

[34] E. Becker, P.-A. Carlsson, M. Skoglundh, Methane oxidation over alumina and ceria supported platinum, Top. Catal. 52 (2009) 1957–1961.

[35] M. Inoue, M. Kimura, T. Inui, Transparent colloidal solution of 2 nm ceria particles, Chem. Commun. (1999) 957–958.

[36] H.P. Klug, L.E. Alexander, X-ray diffraction procedures: for polycrystalline and amorphous materials, John Wiley & Sons, New York, 1974.

[37] A.C. Uribe, G.A.D.A. Montes, G. Torres-Torres, A. Vázquez-Zavala, F. González-García, A. Cordero-García, R. Ojeda-López, Correlation of Rh particle size with CO chemisorption: Effect on the catalytic oxidation of MTBE, J. Compos. Sci. 3 (2019) 81.

[38] K. Arnby, A. Törncrona, B. Andersson, M. Skoglundh, Investigation of Pt/γ-Al$_2$O$_3$ catalysts with locally high Pt concentrations for oxidation of CO at low temperatures, J. Catal. 221 (2004) 252–261.

[39] Asif Jan, Jisu Shin, Junsung Ahn, Sungeun Yang, K. Joong Yoon, Ji-Won Son, Hyoungchul Kim, Jong-Ho Lee, Ho-Il Ji, Promotion of Pt/CeO_2 catalyst by hydrogen treatment for low-temperature CO oxidation, RSC Adv. 9 (2019) 27002–27012.

[40] S. Johansson, L. Österlund, B. Kasemo, CO oxidation bistability diagrams for Pt/CeOx and Pt/SiO2 model catalysts prepared by electron-beam lithography, J. Catal. 201 (2001) 275–285.

[41] J.L. Margitfalvi, I. Borbáth, M. Hegedus, E. Tfirst, S. Gobölös, K. Lázár, Low-temperature CO oxidation over new types of Sn-Pt/SiO$_2$ catalysts, J. Catal. 196 (2000) 200–204.

[42] M. Berdau, G.G. Yelenin, A. Karpowicz, M. Ehsasi, K. Christmann, J.H. Block, Macroscopic and mesoscopic characterization of a bistable reaction system: CO oxidation on Pt(111) surface, J. Chem. Phys 110 (1999) 11551.

[43] A.S. Ivanova, E.M. Slavinskaya, R.V. Gulyaev, V.I. Zaikovskii, O.A. Stonkus, I.G. Danilova, L.M. Plyasova, I.A. Polukhina, A.I. Boronin, Metal-support interactions in Pt/Al$_2$O$_3$ and Pd/Al$_2$O$_3$ catalysts for CO oxidation, Appl. Catal., B 97 (2010) 57–71.

[44] G. Lietz, H. Lieske, H. Spindler, W. Hanke, J. Völter, Reactions of platinum in oxygen- and hydrogen-treated Pt γ-Al$_2$O$_3$ catalysts. II. Ultraviolet-visible studies, sintering of platinum, and soluble platinum, J. Catal. 81 (1983) 17–25.

[45] T. Huizinga, J. Van Grondelle, R. Prins, A temperature programmed reduction study of Pt on Al$_2$O$_3$ and TiO$_2$, Appl. Catal. 10 (1984) 199–213.

[46] A. Aznárez, A. Gil, S.A. Korili, Performance of palladium and platinum supported on alumina pillared clays in the catalytic combustion of propene, RSC Adv. 5 (2015) 82296–82309.

[47] S. Fouladvand, M. Skoglundh, P.-A. Carlsson, A transient in situ infrared spectroscopy study on methane oxidation over supported Pt catalysts, Catal. Sci. Technol. 4 (2014) 3463–3473.

[48] J. Ke, W. Zhu, Y. Jiang, R. Si, Y.J. Wang, S.C. Li, C. Jin, H. Liu, W.G. Song, C.H. Yan, Y.W. Zhang, Strong local coordination structure effects on subnanometer PtO$_x$ clusters over CeO$_2$ nanowires probed by low-temperature CO oxidation, ACS Catal. 5 (2015).

[49] H.H. Liu, Y. Wang, A.P. Jia, S.Y. Wang, M.F. Luo, J.Q. Lu, Oxygen vacancy promoted CO oxidation over Pt/CeO$_2$ catalysts: A reaction at Pt-CeO$_2$ interface, Appl. Surf. Sci. 314 (2014) 725–734.

[50] R. Prins, Hydrogen spillover. Facts and fiction, Chem. Rev. 112 (2012) 2714–2738.

[51] H.C. Yao, Y.F. Yao, Ceria in automotive exhaust catalysts. I. Oxygen storage, J. Catal. 86 (1984) 254–265.

[52] N.M. Martin, M. Skoglundh, G. Smedler, A. Raj, D. Thompsett, P. Velin, F.J. Martinez-Casado, Z. Matej, O. Balmes, P.-A. Carlsson, CO oxidation and site speciation for alloyed palladium–platinum model catalysts studied by in situ FTIR spectroscopy, J. Phys. Chem. C 121 (2017) 26321–26329.

[53] J. Sirita, S. Phanichphant, F.C. Meunier, Quantitative analysis of adsorbate concentrations by diffuse reflectance FT-IR, Anal. Chem. 79 (2007) 3912–3918.

[54] K. Ding, A. Gulec, A.M. Johnson, N.M. Schweitzer, G.D. Stucky, L.D. Marks, P.C. Stair, Identification of active sites in CO oxidation and water-gas shift over supported Pt catalysts, Science 350 (2015) 189–192.

[55] E. Becker, P.-A. Carlsson, L. Kylhammar, M.A. Newton, M. Skoglundh, In situ spectroscopic investigation of low-temperature oxidation of methane over alumina-supported platinum during periodic operation, J. Phys. Chem. C 115 (2011) 944–951.

[56] J. Raskó, CO-induced surface structural changes of Pt on oxide-supported Pt catalysts studied by DRIFTS, J. Catal. 217 (2003) 478–486.

[57] S.K. Cheah, V.P. Bernardet, A.A. Franco, O. Lemaire, P. Gelin, Study of CO and hydrogen on carbon-supported Pt nanoparticles by quadrupole mass spectrometry and operando diffuse reflectance FTIR spectroscopy, J. Phys. Chem. C 117 (2013) 22756–22767.

[58] F. Maugé, C. Binet, J.C. Lavalley, Catalysis by Metals, Springer, Berlin Heidelberg, 1997.

[59] L. Nie, D. Mei, H. Xiong, B. Peng, Z. Ren, X.I.P. Hernandez, A. DeLaRiva, M. Wang, M.H. Engelhard, L. Kovarik, A.K. Datye, Y. Wang, Activation of surface lattice oxygen in single-atom Pt/CeO$_2$ for low-temperature CO oxidation, Science 358 (2017) 1419–1423.

[60] P. Bazin, O. Saur, J.C. Lavalley, M. Daturi, G. Blanchard, FT-IR study of CO adsorption on Pt/CeO$_2$: Characterisation and structural rearrangement of small Pt particles, Phys. Chem. Chem. Phys. 7 (2005) 187–194.

[61] M. Happel, J. Mysliveček, V. Johánek, F. Dvořák, O. Stetsovych, Y. Lykhach, V. Matolín, J. Libuda, Adsorption sites, metal-support interactions, and oxygen spillover identified by vibrational spectroscopy of adsorbed CO: A model study on Pt/ceria catalysts, J. Catal. 289 (2012) 118–126.

[62] A. Bruix, A. Migani, G.N. Vayssilov, K.M. Neyman, J. Libuda, F. Illas, Effects of deposited Pt particles on the reducibility of CeO$_2$(111), Phys. Chem. Chem. Phys. 13 (2011) 11384–11392.

[63] J. Resasco, L. DeRita, S. Dai, J.P. Chada, M. Xu, X. Yan, J. Finzel, S. Hanukovich, A.S. Hoffman, G.W. Graham, et al., Uniformity is key in defining structure–function relationships for atomically dispersed metal catalysts: The case of Pt/CeO$_2$, J. Am. Chem. Soc. 142 (2019) 169–184.

[64] F. Maurer, J. Jelic, J. Wang, A. Gänzler, P. Dolcet, C. Wöll, Y. Wang, F. Studt, M. Casapu, J.-D. Grunwaldt, Tracking the formation, fate and consequence for catalytic activity of Pt single sites on CeO$_2$, Nature Catalysis 3 (2020) 824–833.

[65] F.C. Meunier, L. Cardenas, H. Kaper, B. Šmíd, M. Vorokhta, R. Grosjean, D. Aubert, K. Dembélé, T. Lunkenbein, Synergy between metallic and oxidized Pt sites unravelled during room temperature CO oxidation on Pt/ceria, Angew. Chem. Int. Ed. 60 (2021) 3799–3805.

[66] R. Kopelent, J.A. van Bokhoven, J. Szlachetko, J. Edebeli, C. Paun, M. Nachtegaal, O.V. Safonova, Catalytically active and spectator Ce^{3+} in ceria-supported metal catalysts, Angew. Chem., Int. Ed. 54 (2015) 8728–8731.

[67] S. Gatla, D. Aubert, G. Agostini, O. Mathon, S. Pascarelli, T. Lunkenbein, M.G. Willinger, H. Kaper, Room-temperature CO oxidation catalyst: Low-temperature metal-support interaction between platinum nanoparticles and nanosized ceria, ACS Catal. 6 (2016) 6151–6155.

[68] Y. Lykhach, S.M. Kozlov, T. Skála, A. Tovt, V. Stetsovych, F. Dvořák, V. Johánek, A. Neitzel, J. Mysliveček, S. Fabris, V. Matolín, K.M. Neyman, J. Libuda, Counting electrons on supported nanoparticles, Nat. Mater. 15 (2015) 284–288.

[69] M. Nolan, Y. Lykhach, N. Tsud, T. Skála, T. Staudt, K.C. Prince, V. Matolín, J. Libuda, On the interaction of Mg with the (111) and (110) surfaces of ceria, Phys. Chem. Chem. Phys. 14 (2012) 1293–1301.

[70] G.N. Vayssilov, Y. Lykhach, A. Migani, T. Staudt, G.P. Petrova, N. Tsud, T. Skála, A. Bruix, F. Illas, K.C. Prince, V. Matolín, K.M. Neyman, J. Libuda, Support nanostructure boosts oxygen transfer to catalytically active platinum nanoparticles, Nat. Mater. 10 (2011) 310–315.